Supplemental Data

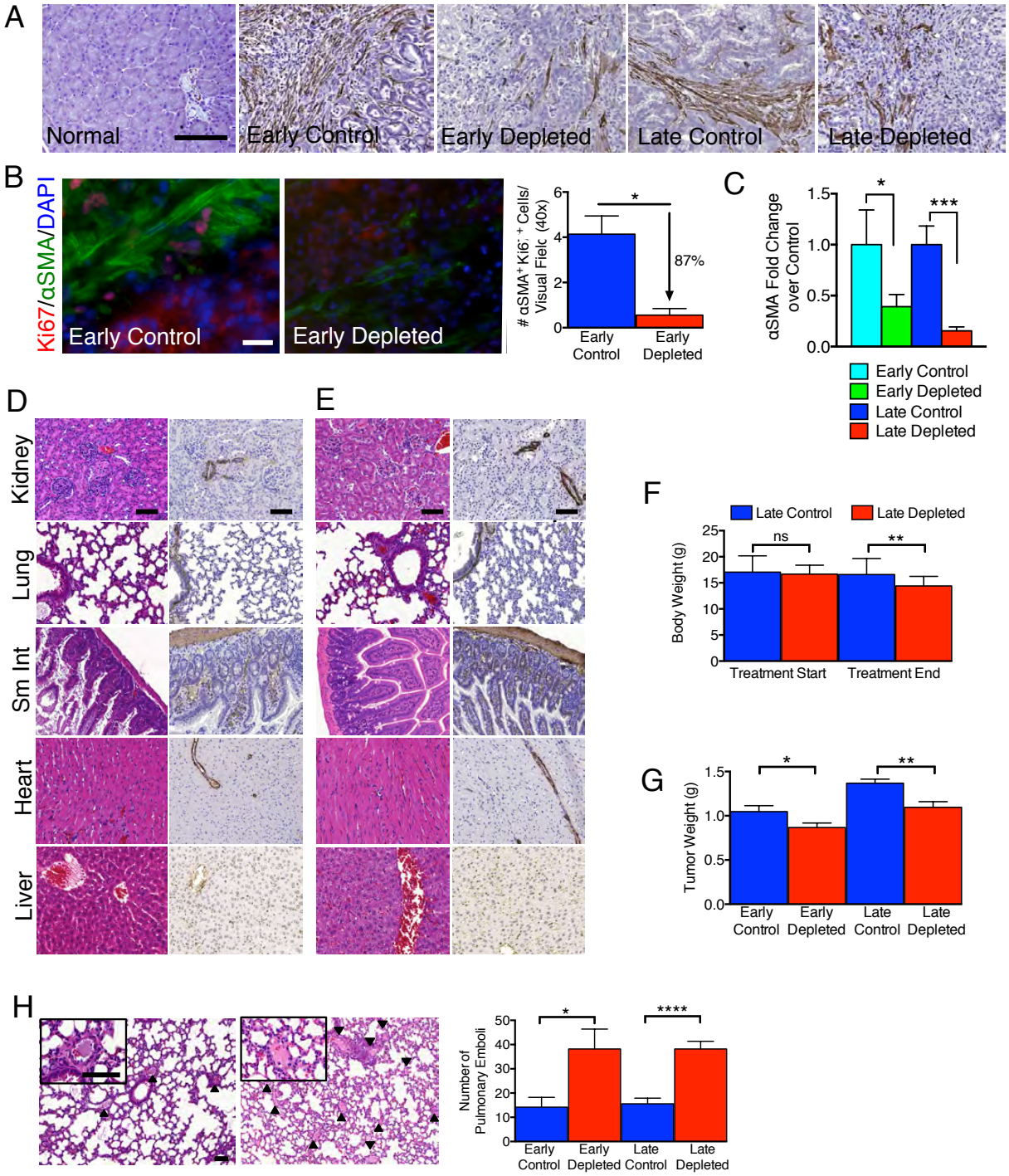

Figure S1, Related to Figure 1. Phenotypic characterization of myofibroblast-depleted tumors from PKT mice

(**A**) Representative micrographs of αSMA stained pancreatic samples (scale bar: 100 μm). (**B**) Representative micrographs (scale bar: 100 μm) of Ki-67/αSMA double-immunofluorescence

and corresponding quantification. Control, n=4; Depleted, n=6. (**C**) Relative αSMA expression in early and late treated PDAC (n=6 in each group). (**D-E**) Representative micrographs of H&E (left) and αSMA (right) stained tissues (scale bar: 100 μm) in Late Control (D) and Late Depleted (E) pancreatic tumor bearing mice. Sm Int: Small intestine. (**F, G**) Body weight (F) at the start and at the end of the treatment and tumor weight (G) at experiment endpoint in the indicated experimental groups. Early Control, n=28; Early Depleted, n=32; Late Control, n=27; Late Depleted, n=25. For body weight, significance was determined by One-way ANOVA with Turkey post-hoc analysis. (**H**) Representative micrographs (scale bar: 400 μm) of lung by H&E with insert at higher magnification (scale bar: 100 μm) from Late Control (left) and Late Depleted (right) mice. Black arrowheads point to pulmonary emboli, and corresponding quantification. Early Control, n=10; Early Depleted, n=10; Late Control, n=14; Late Depleted, n=28. Data is represented as mean +/- SEM. Unless specified otherwise, significance was determined by t-test, * $p<0.05$, ** $p<0.01$, ** $p< 0.001$, **** $p < 0.0001$. ns: not significant.

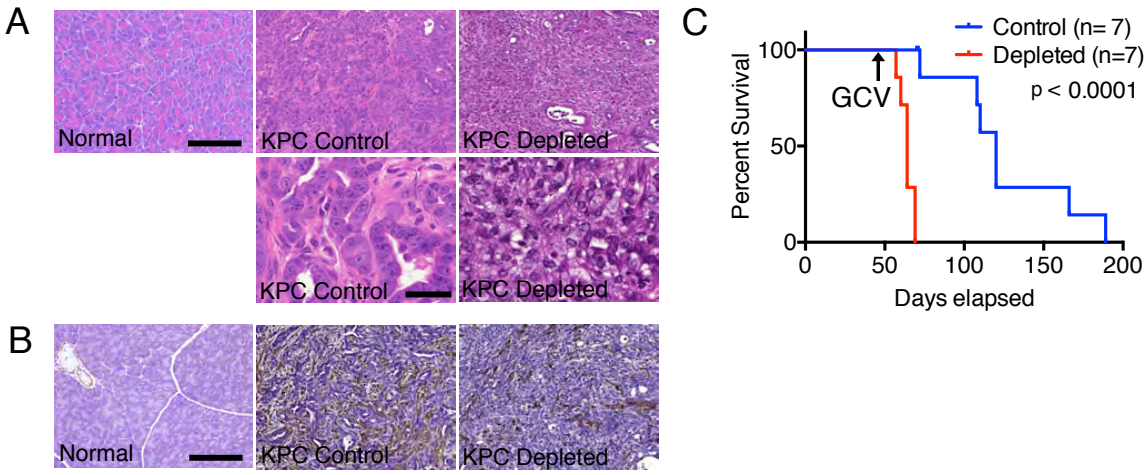

Figure S2, Related to Figure 2. Phenotypic characterization of myofibroblast-depleted tumors from KPC mice

(**A**) Representative micrographs of H&E stained tumors at 88 (Control) and 57 (Depleted) day old mice (top scale bar: 100 μm; bottom scale bar: 50 μm). (**B**) Representative micrographs of αSMA labeled pancreas from the KPC (KPC Control) and KPC; αSMA-tk (KPC Depleted) mice (scale bar: 100 μm). (**C**) Survival analysis of KPC and KPC; αSMA-tk mice. GCV: ganciclovir treatment was initiated. Statistical difference was evaluated using the Log-rank Mantel-Cox test.

Table S1, Related to Figure 2. Patient information

	All	αSMA rich	αSMA poor	p Value
n	53	36	17	
Median age at surgery (range), years	66 (42-84)	65.5 (43-80)	66 (42-84)	
Median survival (range), days	466 (39-2579)	605	310	
Median primary tumor diameter (range), cm	3 (1-6.5)	3 (1-6)	3.5 (1.2-6.5)	
Sex				
Male	31	24	7	0.079
Female	22	12	10	
Ethnicity				
White	48	35	13	0.049
Black	4	1	3	
Other	1	0	1	
Adjuvant Radiation Therapy				
yes	37	26	11	0.04
no	6	6	0	
unknown	10	4	6	
Adjuvant Chemotherapy				
yes	37	26	11	0.04
no	6	6	0	
unknown	10	4	6	
TNM Stage				
T4N1M0	2	1	1	0.59
T3N1M0	42	30	12	
T2N1M0	3	2	1	
T1N1M0	1	1	0	
Unknown	5	2	3	
Stage				
Stage II	46	33	13	0.16
Stage III	3	2	1	
Unknown	4	3	1	
Positive Lymph Node				
Yes	46	33	13	0.302
no	2	1	1	
Unknown	5	2	3	
Vascular Invasion				
yes	22	15	7	0.921
no	26	18	8	
unknown	5	3	2	
Perineural Invasion				
yes	46	30	16	0.25
no	5	5	0	
unknown	2	1	1	
Differentiation				
Well/Moderate	27	22	5	0.031
Poor	26	14	12	

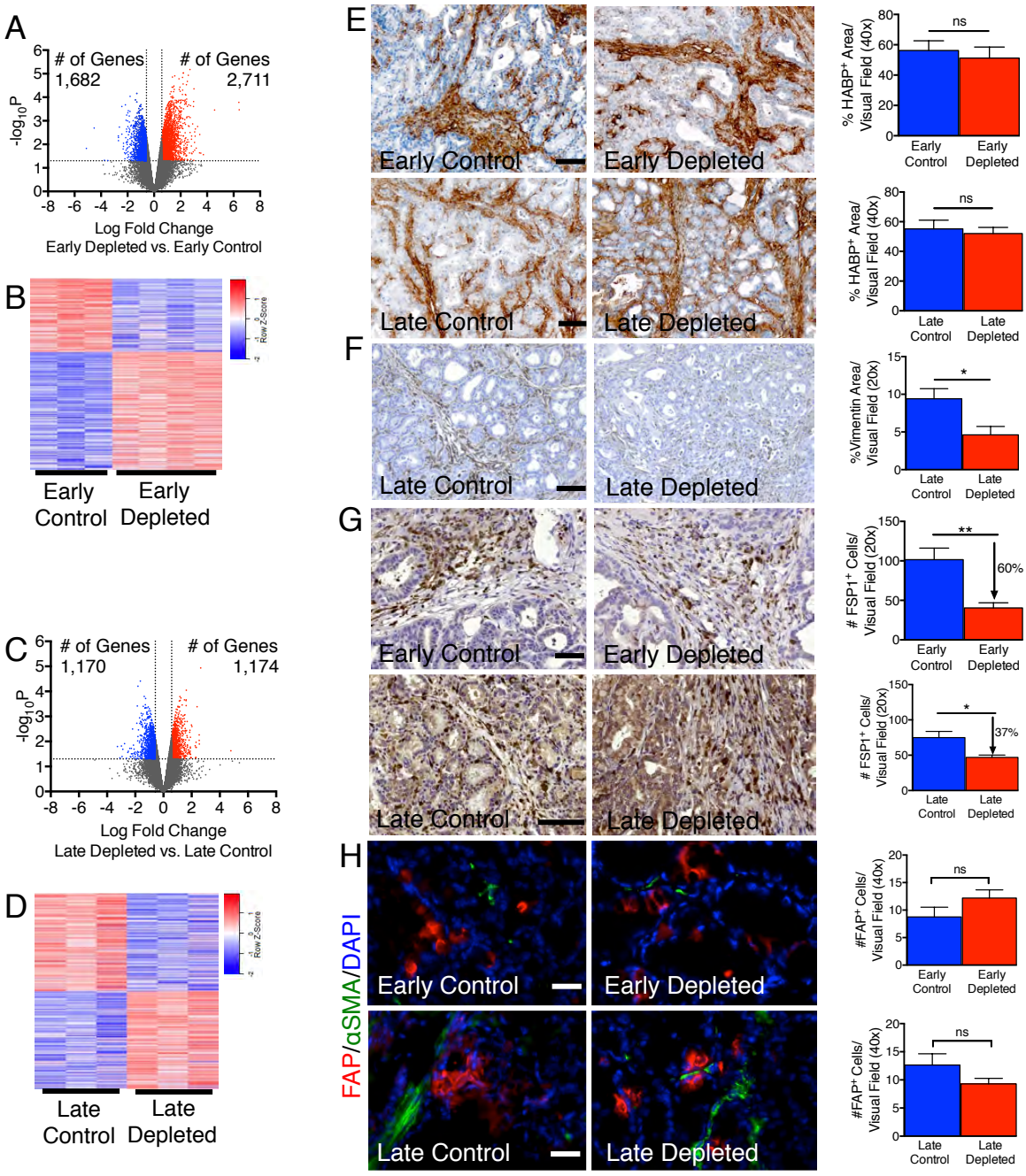

Figure S3, Related to Figure 3. Auditing of mesenchymal cells in myofibroblast-depleted tumors

(**A, B**) Volcano plot (A) of significantly differentiated genes and associated heat map (B) in early depleted PDAC tumors. (**C, D**) Volcano plot (C) of significantly differentiated genes and associated heat map (D) in late depleted PDAC tumors. (**E**) Representative micrographs (scale bar: 50 μm) of HABP IHC and corresponding quantification (n=4 in each group). (**F**)

Representative micrographs (scale bar: 50 μm) of Vimentin IHC and corresponding quantification (n=3 in each group). (**G**) Representative micrographs (scale bar: 100 μm) of FSP1 IHC and corresponding quantification (n=5 in each group). (**H**) Representative micrographs (scale bar: 50 μm) of FAP and αSMA immunostaining and corresponding quantification (n=4 in each group). Data is represented as mean +/- SEM. Significance was determined by t-test, * $p<0.05$, ** $p<0.01$, ** $p< 0.001$, ****$p < 0.0001$. ns: not significant.

Table S2, Related to Figure 3. Ontology analysis based on global gene expression of whole tumors

Selected Gene Ontology Pathways	p Value	Fold Enrichment
Early Depletion		
regulation of chemotaxis	0.00473	3.87028
acute inflammatory regulation	0.03467	3.06220
collagen fibril organization	0.00849	2.84347
actin filament regulation	0.01663	2.79359
collagen metabolic process	0.01551	2.59621
patterning of blood vessels	0.02026	2.48804
vasodilation	0.01411	2.45732
thymus development	0.03749	2.41264
blood vessel remodeling	0.03749	2.41264
neural crest cell migration	0.04711	2.30774
regulation of immune effector process	0.01942	1.65869
positive regulation of immune response	0.00586	1.60991
immune effector process	0.02024	1.52704
angiogenesis	0.02344	1.49656
immune response	0.01283	1.26778
Late Depletion		
fibril organization	0.01813	12.50046
regulation of VEGFR signaling pathway	0.03434	9.37534
regulation of macrophage activation	0.01395	7.14312
regulation of T cell mediated cytotoxicity	0.00848	5.68203
thymic T cell selection	0.00492	5.00018
antigen processing and presentation of peptide antigen via MHC class II	0.03397	3.90639
regulation of mesenchymal cell proliferation	0.03238	3.26099
positive regulation of T cell differentiation	0.01169	3.12511
regulation of leukocyte mediated cytotoxicity	0.02901	2.91677
regulation of interferon-gamma production	0.03869	2.73448
T cell differentiation in the thymus	0.03869	2.73448
positive regulation of cell adhesion	0.01907	2.61638
B cell activation	0.04519	1.92315
regulation of cell adhesion	0.03591	1.86177
regulation of leukocyte activation	0.03821	1.62343

Associated Pathways: EMT/Migration Angiogenesis Immunity

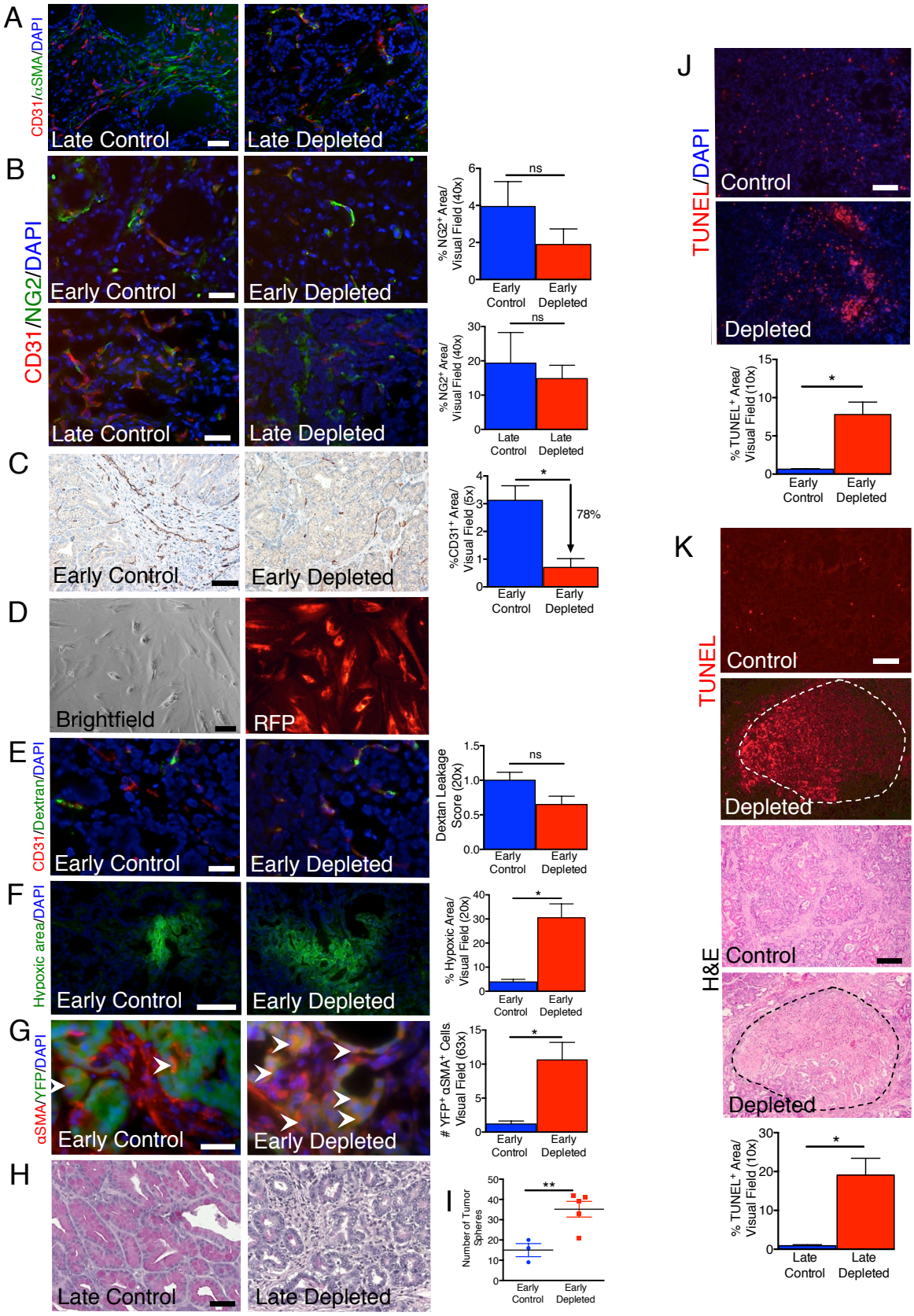
A
CD31/αSMA/DAPI
Late Control
Late Depleted
B
CD31/NG2/DAPI
Early Control
Early Depleted
Late Control
Late Depleted
% NG2+ Area/ Visual Field (40x)
ns
Early Control
Early Depleted
% NG2+ Area/ Visual Field (40x)
ns
Late Control
Late Depleted
C
Early Control
Early Depleted
%CD31+ Area/ Visual Field (5x)
*
78%
Early Control
Early Depleted
D
Brightfield
RFP
E
CD31/Dextran/DAPI
Early Control
Early Depleted
Dextan Leakage Score (20x)
ns
Early Control
Early Depleted
F
Hypoxic area/DAPI
Early Control
Early Depleted
% Hypoxic Area/ Visual Field (20x)
*
Early Control
Early Depleted
G
αSMA/YFP/DAPI
Early Control
Early Depleted
YFP+ αSMA+ Cells Visual Field (63x)
*
Early Control
Early Depleted
H
Late Control
Late Depleted
I
Number of Tumor Spheres
**
Early Control
Early Depleted
J
TUNEL/DAPI
Control
Depleted
% TUNEL+ Area/ Visual Field (10x)
*
Early Control
Early Depleted
K
TUNEL
Control
Depleted
H&E
Control
Depleted
% TUNEL+ Area/ Visual Field (10x)
*
Late Control
Late Depleted

Figure S4, Related to Figure 4. Invasive properties and enhanced apoptosis in tumors with early depletion of myofibroblasts

(**A**) Representative micrographs of CD31 and αSMA immunostaining (scale bar: 100 μm). (**B**) Representative micrographs (scale bar: 50 μm) of CD31 and NG2 immunostaining and corresponding quantification (n=3 in each group). (**C**) Representative micrographs (scale bar: 100 μm) of CD31 IHC and corresponding quantification. Control, n=4; Depleted, n=3. (**D**) Brightfield and red fluorescent protein (RFP) imaging of αSMA-RFP$^+$ myofibroblasts from mouse PDAC tumor (scale bar: 50 μm). (**E**) Representative micrographs (scale bar: 100 μm) of CD31 cells in tumors post FITC-Dextran injection and corresponding quantification. Control, n=3; Depleted, n=4. (**F**) Representative micrographs (scale bar: 100 μm) of hypoxia indicator, Hypoxyprobe™, and corresponding quantification. Control, n=4; Depleted, n=3. (**G**) Representative micrographs (scale bar: 50 μm) of αSMA$^+$ cells in tumors with YFP$^+$ linage tagged cancer cells and corresponding quantification of dual positive cells (n=4 in each group). White arrowheads point to dual positive αSMA$^+$YFP$^+$ cancer cells. (**H**) Representative micrographs of mucin (mucicarmine) stained tumors (scale bar: 100 μm) from late control and late depleted tumors. (**I**) Quantitation of YFP$^+$ tumor sphere formation from early control and early depleted tumors. (**J**) Representative micrographs of the apoptosis marker TUNEL (scale bar: 200 μm) from early control and early depleted tumors and corresponding quantification (n=3 in each group). (**K**) Representative micrographs of the apoptosis marker TUNEL (scale bar: 200 μm) from late control and late depleted tumors, matched H&E staining, and corresponding quantification (n=3 in each group). The differentiated islet is encircled. Data is represented as mean +/- SEM. Significance was determined by t-test, * $p<0.05$, ** $p<0.01$, ** $p< 0.001$, **** $p < 0.0001$. ns: not significant.

Table S3, Related to Figure 4. Ontology analysis based on global gene expression of normal pancreas and tumor associated myofibroblasts.

Selected Gene Ontology Pathways	p Value	Fold Enrichment
Illumina		
Regulation of T cell mediated cytotoxicity	0.03942	1.61646
T cell receptor signaling pathway	0.03902	1.39604
actin filament organization	0.00235	1.32781
immune response-activating cell surface receptor signaling pathway	0.02113	1.30106
regulation of cell migration	0.00057	1.28263
T cell differentiation	0.00249	1.27616
cell-substrate adhesion	0.02157	1.24780
T cell activation	0.00185	1.22628
regulation of cell adhesion	0.02142	1.18655
leukocyte differentiation	0.00473	1.18389
extracellular structure organization	0.00403	1.18251
angiogenesis	0.00786	1.17893
blood vessel development	0.00043	1.17260
vasculature development	0.00071	1.16385
positive regulation of immune system process	0.00253	1.16134
blood vessel morphogenesis	0.00347	1.15928
lymphocyte activation	0.00980	1.14253
biological adhesion	0.00001	1.14188
cell-cell adhesion	0.00559	1.13700
immune system development	0.00344	1.12879
inflammatory response	0.01115	1.12793
cytoskeleton organization	0.00540	1.11566
cell motility	0.00941	1.11559
cell motion	0.00668	1.10554
immune response	0.00223	1.10510
response to wounding	0.01246	1.09938
RNA-Seq		
T cell costimulation	0.03540	3.59091
lymphocyte costimulation	0.03540	3.59091
positive regulation of B cell proliferation	0.00813	2.61157
positive regulation of cell-substrate adhesion	0.00366	2.55354
vasodilation	0.01194	2.34074
response to hypoxia	0.00010	2.24432
response to oxygen levels	0.00013	2.20979
cell-matrix adhesion	0.00161	2.20039
regulation of blood vessel size	0.00029	2.15455
vascular process in circulatory system	0.00101	2.07213
blood coagulation	0.00157	1.97232
extracellular matrix organization	0.00153	1.94213
actin cytoskeleton organization	0.00000	1.91515
response to wounding	0.00000	1.83984
inflammatory response	0.01452	1.81435
positive regulation of leukocyte proliferation	0.00579	1.76783
blood circulation	0.01610	1.76070
circulatory system process	0.00093	1.75987
blood vessel development	0.00014	1.74693
vasculature development	0.01897	1.73276
positive regulation of lymphocyte proliferation	0.00807	1.72364
immune response	0.00000	1.65945
acute inflammatory response	0.00000	1.63241
regulation of cell migration	0.03455	1.62931
angiogenesis	0.00509	1.56310
vessel morphogenesis	0.02414	1.54002

Assocated pathways: EMT/migration/ECM remodling, Angiogenesis, Immunity

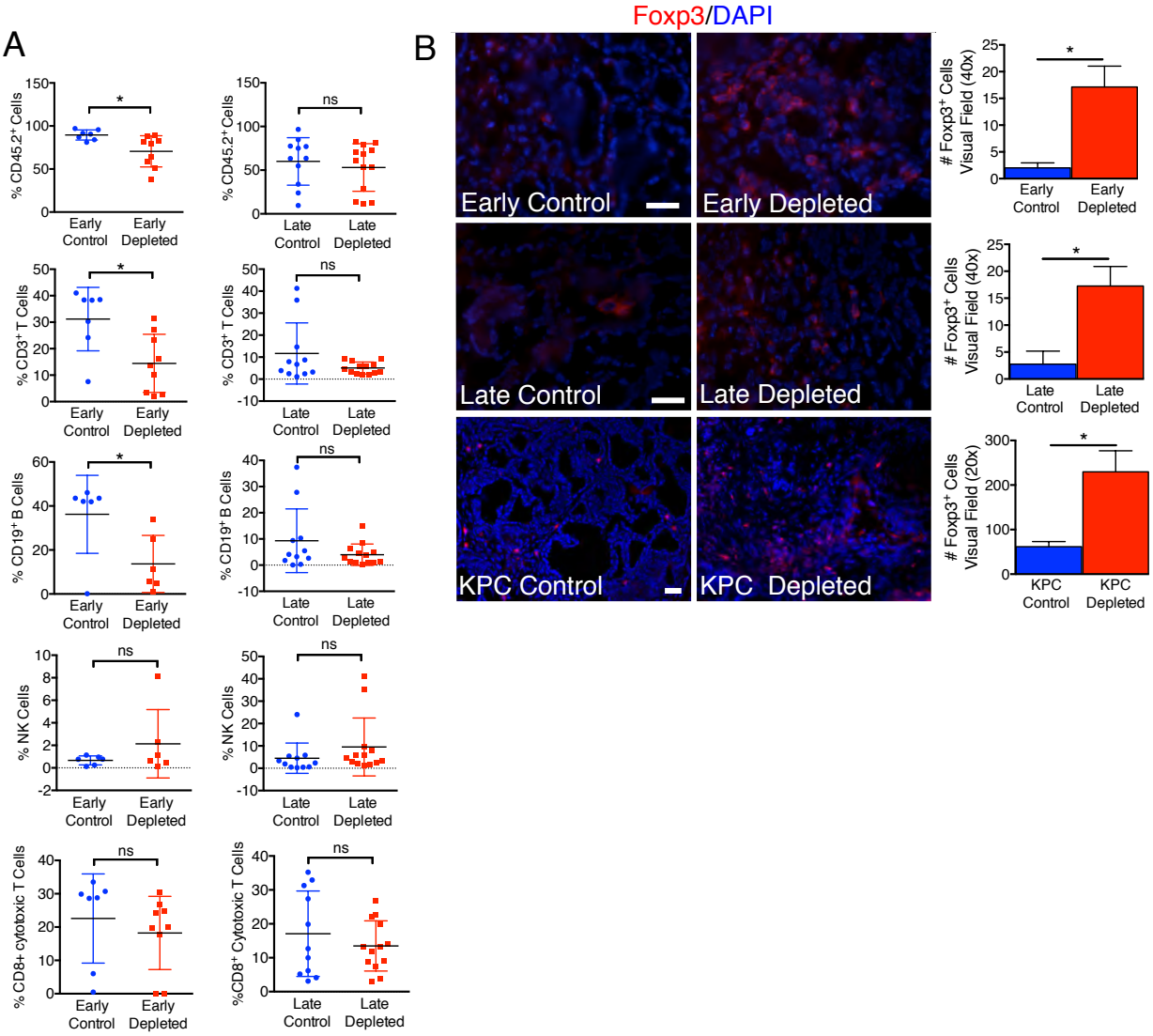

Figure S5, Related to Figure 6. Auditing of immune infiltration in myofibroblast-depleted tumors

(**A**) Tumor immune infiltrate composition assayed by flow cytometry analysis in early (left) and late (right) control and depleted tumors. (**B**) Representative micrographs (scale bar: 50 μm) for Foxp3 immunostaining and corresponding quantification. Early Control, n=6; Early Depleted, n=4; Late Control, n=4; Late Depleted, n=3; KPC Control, n=3; KPC Depleted n=3. Data is represented as mean +/- SEM. Unless otherwise noted, significance was determined by t-test, * $p<0.05$, ** $p<0.01$, ** $p< 0.001$, ****$p < 0.0001$. ns: not significant.

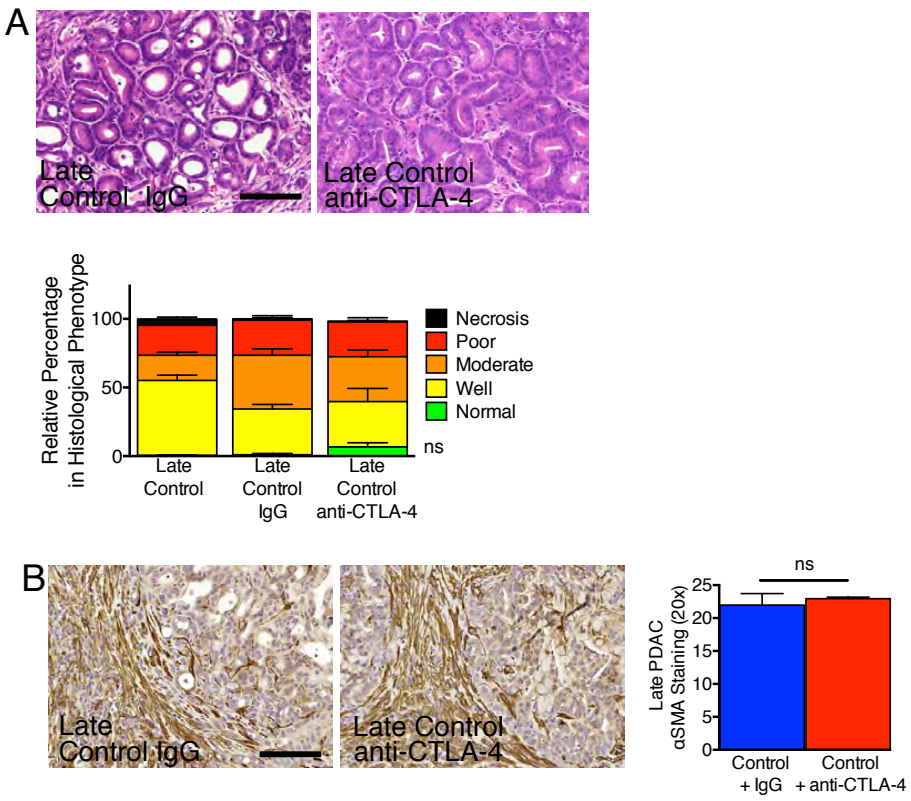

Figure S6, Related to Figure 7.

(**A**) Representative micrographs of H&E stained pancreatic samples (scale bar: 100 μm) and percent tissue encompassed by each pathological hallmark. Late Control, n=15; Late Control + IgG, n=5; Late Control + anti-CTLA-4, n=4. Significance was determined by One-way ANOVA with Turkey post-hoc analysis. (**B**) Representative micrographs of αSMA stained pancreatic samples (scale bar: 100 μm) and corresponding quantification. Late Control, n= 4; Late Control+ anti-CTLA-4, n=5. Data is represented as mean +/- SEM. Unless otherwise noted, significance was determined by t-test, * $p<0.05$, ** $p<0.01$, ** $p< 0.001$, ****$p < 0.0001$. ns: not significant.

Supplemental Experimental Procedures

Acquisition and analysis of ^{18}F-FDG PET/CT in mice

Mice were fasted for 4 hours prior to imaging and were kept warm using heating pads. Animals were anesthetized with 2% isoflurane and 100% oxygen, and 400-500 μCi of ^{18}F-FDG was injected to each mouse via the lateral tail veins using a 30-gauge catheter. One hour later, static PET dataset for each mouse was acquired on an Argus microPET/CT scanner (Sedecal Inc., Spain) for 10 minutes in 2 bed positions using an energy window of 250-700 keV. Images were reconstructed using a 2D OSEM algorithm with 2 iterations and 16 subsets. For measuring the mean and maximum standardized uptake values (SUVmean and SUVmax), three-dimensional (3D) regions of interest were drawn over the tumors and uptake values were measured using the Argus software (Sedecal Inc., Spain). CT scans were acquired following PET imaging in standard resolution. The scan parameters were set as follows: 40 kVp tube voltage, 140 μA tube current, 360 projections, number of shots 8, axial field-of-view 80 mm. Scans were recorded without respiratory gating, and image data were reconstructed using the FeldKemp algorithm.

Fibroblast culture from mouse tumors and normal pancreas

Tumors and normal pancreas were excised and washed with PBS, transferred to a 10 cm^2 tissue culture plate, minced, digested with 400 U/ml type IV collagenase and 0.2 mg/ml DNase I in RPMI supplemented with 1% PSA at 37°C overnight. The next day the digested tissue was spun down and plated back with 20% FBS/RPMI, and myofibroblasts were allowed to grow until confluent.

Atomic force microscopy

Frozen tissue blocks were cut into 20 μm thick sections. Prior to the atomic force microscopy (AFM) measurement, each section was immersed in PBS and thawed at room temperature. The samples were maintained in proteinase inhibitor in PBS (protease inhibitor cocktail, Roche

Diagnostics, 11836170001) supplemented with Propidium Iodide (SIGMA P4170, 20 μg/ml) during the AFM session. Three mice for each group were used for AFM quantification of Young's elastic modulus of the cancer-associated stroma. AFM indentations were performed using an MFP3D-BIO inverted optical AFM (Asylum Research) mounted on a Nikon TE2000-U inverted fluorescent microscope, as previously described (Lopez et al., 2011). Briefly, we used silicon nitride cantilevers with spring constant of 0.06 N/m with borosilicate glass spherical tip with 5 μm in diameter (Novascan Tech). The cantilever was calibrated using the thermal oscillation method prior to each experiment. Samples were indented at a 20 μm/s loading rate, with a maximum force of 2 nN. Five AFM force maps were typically obtained on each sample, each map as a 10x10 μm raster series of indentations utilizing the FMAP function of the IGOR PRO build supplied by Asylum Research. The Hertz model was used to determine the elastic properties of the tissue (E1). Tissue samples were assumed to be incompressible and a Poisson's ratio of 0.5 was used in the calculation of the Young's elastic modulus.

Collagen content and cross-linking

Frozen pancreatic tissues were reduced with standardized NaB3H4, hydrolyzed with 6N HCl, and total collagen content was quantified in the hydrolysate by hydroxyproline content measured by amino acid analysis, and equal amount of hydroxyproline was applied to an ion exchange HPLC. The content of reducible cross-links and aldehydes as their reduced forms based on the specific activity of NaB3H4 was then determined by quantifying the fluorescent cross-links (pyridinoline and deoxypyridinoline) as an integration of the areas of the respective fluorescent peaks, standardized by the hydrolysate of an apparently pure pyridinoline containing peptides. The cross-links and cross-link precursor aldehydes were then calculated as a mole/mole of collagen basis based on the value of 300 residues of hydroxyproline per collagen molecule (Yamauchi and Shiiba, 2008).

Quantitative real-time PCR

All procedures were performed as previously described (Cooke et al., 2012). Primer sequences are listed below.

Gene	Sequence
ARP/36b4	F 5'-GGAGCCAGCGAGGCCACACTGCTG-3' R 5'-CTGGCCACGTTGCGGACACCCTCC-3'
αSMA (*Acta2*)	F 5'-GTCCCAGACATCAGGGAGTAA-3' R 5'-TCGGATACTTCAGCGTCAGGA-3'
Twist	F 5'-CGGGAGTCCGCAGTCTTA-3' R 5'-TGAATCTTGCTCAGCTTGTC-3'
Snail	F 5'-GCGGAAGATCTTCAACTGCAAATATTGTAAC-3' R 5'-GCAGTGGGAGCAGGAGAATGGCTTCTCAC-3'
Slug	F 5'-CACATTCGAACCCACACATTGCCT-3' R 5'-TGTGCCCTCAGGTTTGATCTGTCT-3'
18S	F 5'-GTAACCCGTTGAACCCCATT-3' R 5'-CCATCCAATCGGTAGTAGCG-3'
Ctla4	F 5'-CCTTTAATGAAAGCAGAGTGAACC-3' R 5'- ATCTTGCTCAAAGAAACAGCAG-3'

Supplemental References

Lopez, J.I., Kang, I., You, W.K., McDonald, D.M., and Weaver, V.M. (2011). In situ force mapping of mammary gland transformation. Integr Biol (Camb). *3*, 910-921.

Yamauchi, M., and Shiiba, M. (2008). Lysine hydroxylation and cross-linking of collagen. Methods Mol Biol. *446*, 95-108.